ADVANCED THEORY AND SIMULATIONS
www.advtheorysimul.com

Controlling Chemical Waves by Transforming Transient Mass Transfer

Zeren Zhang, Liujun Xu, and Jiping Huang**

Manipulating transient mass transfer plays a crucial role in physics, chemistry, biology, and other fields. One typical example is chemical waves, whose concentration profiles have spatiotemporal variations. Based on a general model associated with the advection-diffusion equation, an optimized transformation-mass-transfer theory is proposed to flexibly control transient mass transfer. As an example application, a class of separators is theoretically designed to achieve the separation of chemical waves. Meanwhile, three typical types of devices for cloaking, concentrating, and rotating chemical waves are proposed successfully, thus offering more versatile control methods. Such theoretical analysis is well confirmed by the computer simulations. These results provide insights into novel manipulation of chemical waves associated with biochemical reactions and promote potential applications for transient mass diffusion.

1. Introduction

Precise manipulation of mass transfer is particularly important to biochemical reactions, medicine deliveries, and separation membranes, among others.[1] For example, some drug components only work for a special target cell, but in most cases the medicine particles are absorbed by irrelevant cells or react with other chemical components during delivery in the blood, which always compromises therapeutic efficacy. Thus, a great deal of researches aim to control drug mobility.[2,3] For another example, particle separation, focusing, and detection are common fundamental operations in industry and biochemistry, including but not limited to manufacturing fossil fuels from crude oil, harvesting uranium from seawater, and monitoring harmful solutes in gases or liquids.[4–7] From a physical point of view, mass transfer is essentially governed by an advection-diffusion equation. Based on this equation,[8,9] many physical approaches, including the scattering-cancellation method and transformation theory, were proposed to control mass transfer.[10–14]

However, when it comes to mass-transfer manipulation in transient (or time-dependent) states, the case becomes very different. A typical example of broad concern is chemical waves.[15–23] In simple terms, chemical waves, driven far from equilibrium, feature concentration profiles with spatiotemporal variations, which are completely transient problems. Unfortunately, transient mass transfer generally does not have the property of form-invariance under coordinate transformations, so the existing transformation theory is not applicable. Although transient light transport and heat diffusion may provide some insights,[24–28] the related approaches are restricted to certain geometries or transformations. Therefore, the relevant theories are still confronted with big challenges to control chemical waves.

To solve the problem, we established an optimized transformation-mass-transfer theory that enabled us to flexibly manipulate chemical waves and analyze their propagation properties. We further designed four representative devices that were used for cloaking, concentrating, rotating, and separating chemical waves, respectively. See **Figure 1**. Here, "cloaking" means a zero-concentration gradient inside the device; "concentrating" indicates a larger concentration gradient inside the device; "rotating" refers to propagation deflecting of waves inside the device, and "separating" represents the separation of different particle-concentration waves. Most importantly, all four devices did not disturb the wave profiles in the background. Our results may broaden the horizon of manipulating transient mass transfer and may be helpful to trigger new applications of chemical waves. The next section will introduce the theory behind this.

2. Results and Discussion

2.1. Modeling Chemical Waves

Despite a chemical process, we disregarded specific chemical components and instead assumed that concentration gradients were the main driving forces. Therefore, we could apply an advection-diffusion equation to describe chemical waves[29–31]

$$\frac{\partial c}{\partial t} = \nabla \cdot \left(\overleftrightarrow{D} \cdot \nabla c - \nu c \right) \tag{1}$$

where c, t, $\overleftrightarrow{D}$, and ν are concentration, time, tensorial diffusivity, and advection velocity, respectively. The key physical meaning of Equation (1) is mass conservation. Without loss of generality, we

Z. Zhang, L. Xu, J. Huang
Department of Physics, State Key Laboratory of Surface Physics, and Key Laboratory of Micro and Nano Photonic Structures (MOE)
Fudan University
Shanghai 200438, China
E-mail: 13307110076@fudan.edu.cn; jphuang@fudan.edu.cn

The ORCID identification number(s) for the author(s) of this article can be found under https://doi.org/10.1002/adts.202100375

DOI: 10.1002/adts.202100375

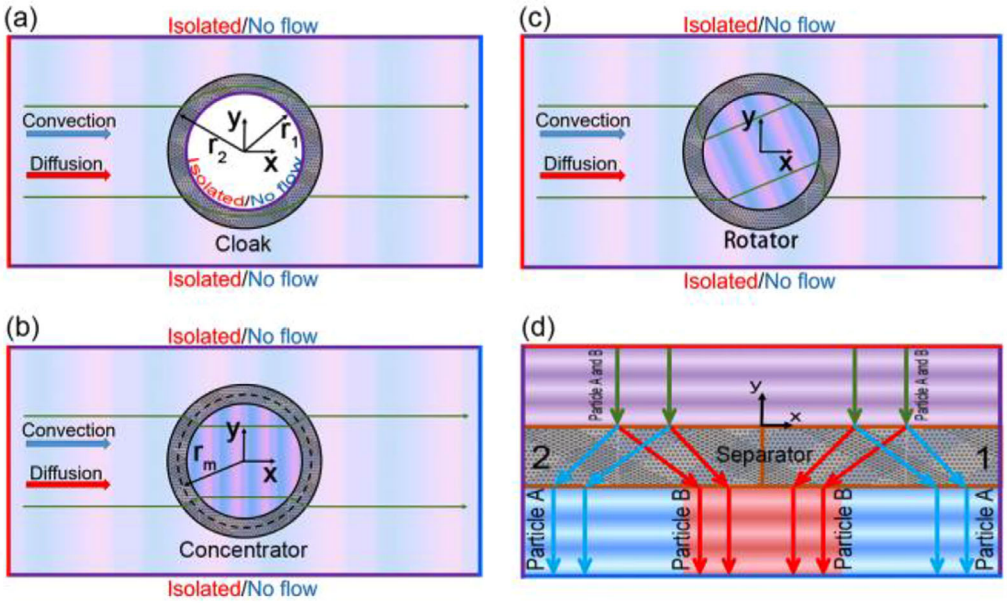

Figure 1. a–d) Schematic diagrams of cloaking, concentrating, rotating, and separating in two dimensions, respectively. In (a)–(c), the length and height of the rectangle were $u_1 = 0.2$ m and $u_1 = 0.1$ m, respectively. In (d), we set length $m_1 = 0.014$ m, and height $m_2 = 0.009$ m. The initial particle concentration for (a)–(d) was set as $c_0 = 0$ mol m^{-3}.

considered a 1D case with a scalar diffusivity D and a constant velocity v along the x-axis. Therefore, Equation (1) could be reduced to

$$\frac{\partial c}{\partial t} = D\frac{\partial^2 c}{\partial x^2} - v\frac{\partial c}{\partial x} \tag{2}$$

For a chemical wave, its concentration varies spatiotemporally, so it is reasonable to use a plane-wave solution

$$c = c_a e^{i(\beta x - \omega t)} + c_r \tag{3}$$

where c_a, β, ω, and c_r are the concentration amplitude, wave number, circular frequency, and reference concentration of the chemical wave, respectively. Since the frequency of the concentration source was preset, the concentration amplitude of the chemical wave decreased along the propagation direction, which caused a complex wave number $\beta = k + i\alpha$ with k and α being two real numbers. Therefore, Equation (3) could also be written as $c = c_a e^{-\alpha x} e^{i(kx-\omega t)} + c_r$. Clearly, α represents the spatial dissipation of the chemical wave and k is the real wave number. Its substitution into Equation (2) yields

$$\alpha = \frac{-2v + \xi}{4D} \tag{4a}$$

$$k = \frac{\sqrt{v^4 + 16D^2\omega^2} - v^2}{16D^2\omega}\xi \tag{4b}$$

with $\xi = \sqrt{2v^2 + 2\sqrt{v^4 + 16D^2\omega^2}}$. Here we only concerned about forward propagation. That was why we kept the positive solution. The $\alpha - \omega$ and $k - \omega$ curves are shown in the inset of **Figure 2**. Clearly, a larger ω leads to a larger α or k. Such a concentration

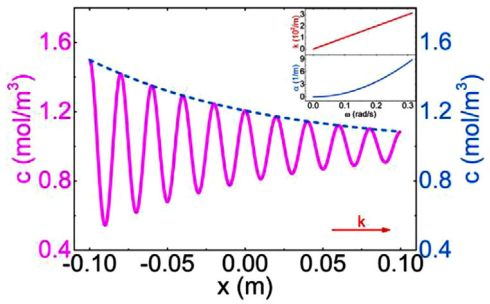

Figure 2. Particle concentration (c) distribution along x-axis. Blue dashed line indicates the dissipation trend of chemical wave. Red arrow denotes the direction of propagation. Inset shows the real and imaginary part of wave number, k and α, as a function of ω, respectively.

profile can be approximately regarded as a chemical wave. Nevertheless, a rigorous model of chemical waves was more complicated than the present one,[13] but to some extent, our efforts could provide different guidance to control chemical waves with the following optimized-transformation theory for transient mass transfer.

2.2. Optimized-Transformation Transient-Mass-Transfer Theory

To obtain the transformation rule, we wrote down the component form of the advection-diffusion equation in a curvilinear space with the corresponding coordinate x_i

$$\sqrt{G}\partial_t c = \partial_i\left(\sqrt{G}D^{ij}\partial_j c - \sqrt{G}v_i c\right) \tag{5}$$

where G is the determinant of $G_i \cdot G_j$, with G_i and G_j being covariant bases of the curvilinear space. We then expressed Equation (5) in the physical space x_i' as

$$\sqrt{G}\partial_t c = \partial_{i'}\frac{\partial x_i'}{\partial x_i}\left(\sqrt{G}D^{ij}\frac{\partial x_j'}{\partial x_j}\partial_{j'}c - \sqrt{G}v_i c\right) \tag{6}$$

where $\partial x_i'/\partial x_i$ and $\partial x_j'/\partial x_j$ are just the components of the Jacobian-transformation matrix J whose determinant det$J$ is equal to $1/\sqrt{G}$. Therefore, Equation (6) could be reduced to

$$\frac{1}{\det J}\partial_t c = \nabla' \cdot \left(\frac{\overleftrightarrow{JDJ^\tau}}{\det J}\cdot\nabla' c - \frac{Jv}{\det J}c\right) \tag{7}$$

where J^τ is the transpose of J. Unfortunately, if we denoted the transformed parameters $\frac{\overleftrightarrow{JDJ^\tau}}{\det J}$ and $\frac{Jv}{\det J}$ as $\overleftrightarrow{D}''$ and v'', the space transformation could not be completely replaced by the material transformation due to the lack of a physical quantity in front of $\partial_t c$. Therefore, transient mass transfer does not have form-invariance under a coordinate transformation except for when det $J = 1$.

To solve the problem, we took an approximation to remove the $1/\det J$ in front of $\partial_t c$ and rewrote Equation (7) as

$$\partial_t c = \nabla' \cdot \left(\overleftrightarrow{JDJ^\tau}\cdot\nabla' c - Jvc\right) \tag{8}$$

We emphasized that Equation (8) is generally an approximate version of Equation (7) because det J is a position-dependent quantity. Fortunately, our following simulations showed that the approximation was completely feasible. Therefore, the transformed parameters $\overleftrightarrow{D}'$ and v' could be summarized as

$$\overleftrightarrow{D}' = \overleftrightarrow{JDJ^\tau} \tag{9a}$$

$$v' = Jv \tag{9b}$$

Then the Equation (8) could keep form invariant approximately under coordinate transformation. Since Equation (9) performed well in simulations, it corresponded to the optimized transformation-mass-transfer theory. Meanwhile, Equation (9) was different from the reduced parameters derived by dividing det$J$ to remove infinite parameters.[32–34] Furthermore, the optimization presented in Equation (9) was crucially different from topology optimization.[35–37]

2.3. Four Model Applications

As practical applications of our optimized transformation-mass-transfer theory, we further designed four functional devices to achieve cloaking, concentrating, rotating, and separating of chemical waves, as shown in Figure 1. It can be seen from Figure 1a–c that the chemical waves propagated from left side to right side and flowed through the devices without changing wave profiles. Cloaking can protect the object in the core region, while concentrating can increase the particle-concentration gradient in the core region. Rotating can flexibly control the propagation direction of chemical waves. We will introduce the cloak first.

The coordinate transformation of cloaking from a virtual space (r, θ) to the physical space (r', θ') can be expressed as $r' = ar + b$ and $\theta' = \theta$ with $a = (r_2 - r_1)/r_2$ and $b = r_1$. Here, r_1 and r_2 are the radii of the inner and outer boundaries of the cloak, respectively (Figure 1a). The Jacobian transformation matrix J can be calculated as J=diag$[a r',\ a/(r' - b)]$. Therefore, according to Equation (9), the transformed parameters $\overleftrightarrow{D}'$ and v' become

$$\overleftrightarrow{D}' = \begin{bmatrix} D_0 a^2 & 0 \\ 0 & D_0(r'\ a/\ (r' - b))^2 \end{bmatrix} \tag{10a}$$

$$v' = \begin{bmatrix} v_r a \\ v_t r'\ a/\ (r' - b) \end{bmatrix} \tag{10b}$$

where D_0 and $v_0 = [v_r,\ v_t]^\tau$ are the diffusivity and advection velocity of the background, respectively. Indeed, there might be some discontinuity for fluid in the medium. But this problem can be solved by active control of flow on the boundary. According to Equation (10), we could achieve cloaking of chemical waves.

For a concentrator, the coordinate transformation becomes $r' = hr$ for $r < r_m$, $r' = nr + m$ for $r_m < r < r_2$, and $\theta' = \theta$ for $0 < r < r_2$, where $h = r_1/r_m$, $n = (r_2 - r_1)/(r_2 - r_m)$, $m = (r_1 - r_m)r_2/(r_2 - r_m)$, and r_m is a radius between r_1 and r_2 (the dashed line in Figure 1b). Therefore, the Jacobian-transformation matrices of the concentrator are J_1=diag$[h, h]$ for the region $r' < r_1$ and J_2=diag$[n, r'n/(r' - m)]$ for the region $r_1 < r' < r_2$. We then expressed the transformed parameters in the region $r' < r_1$ (i.e., $\overleftrightarrow{D}_1'$ and v_1') and those in the region $r_1 < r' < r_2$ (i.e., $\overleftrightarrow{D}_2'$ and v_2') as

$$\overleftrightarrow{D}_1' = \begin{bmatrix} D_0 h^2 & 0 \\ 0 & D_0 h^2 \end{bmatrix} \tag{11a}$$

$$v_1' = \begin{bmatrix} v_r h \\ v_t h \end{bmatrix} \tag{11b}$$

$$\overleftrightarrow{D}_2' = \begin{bmatrix} D_0 n^2 & 0 \\ 0 & D_0(r'\ n/\ (r' - m))^2 \end{bmatrix} \tag{12a}$$

$$v_2' = \begin{bmatrix} v_r n \\ v_t r'\ n/\ (r' - m) \end{bmatrix} \tag{12b}$$

The reciprocal of h (i.e., r_1/r_m) determines the concentrating effect. That is, a bigger r_m leads to a higher concentrating effect, and the maximum value is r_2/r_1. Here we set $r_2 = 0.035$ m, $r_m = 0.03$ m, $r_1 = 0.025$ m, $D_0 = 9 \times 10^{-8}$ m s^{-1}, $v_0 = [10^{-3},\ 0]^\tau$ m s^{-1}, and $\theta_0 = \pi/6$. The slow velocity v_0 was set to ensure creeping flow and avoid turbulent flow and the value of D_0 was close to real diffusion value (for example, diffusivity of O_2 in PDMS equals 3.4×10^{-9} m s^{-1}).

Note that the above coordinate transformations only stretch or compress the radius without transforming the angle. Thus, we applied the optimized theory to rotate the chemical waves. The coordinate transformation of rotating obeys $r' = r$ for the region $0 < r < r_2$, $\theta' = \theta + \theta_0$ for the region $r < r_1$, and $\theta' = \theta + g(r - r_2)$ for the region $r_1 < r < r_2$ (Figure 1c). Here, $g = \theta_0/(r_1 - r_2)$, and

θ_0 is a rotation angle. We then derived the Jacobian transformation matrices: J_1 is a unit matrix for the region $r' < r_1$, and J_2=[(1, 0), ($r'g$, 1)] for the region $r_1 < r' < r_2$. Therefore, the transformed parameters in the region $r' < r_1$ (i.e., $\overleftrightarrow{D}_1'$ and v_1') and those in the region $r_1 < r' < r_2$ (i.e., $\overleftrightarrow{D}_2'$ and v_2') are

$$\overleftrightarrow{D}_1' = \begin{bmatrix} D_0 & 0 \\ 0 & D_0 \end{bmatrix} \tag{13a}$$

$$v' = \begin{bmatrix} v_r \\ v_t \end{bmatrix} \tag{13b}$$

$$\overleftrightarrow{D}_2' = \begin{bmatrix} D_0 & D_0 r' g \\ D_0 r' g & D_0 \left[(r' g)^2 + 1 \right] \end{bmatrix} \tag{14a}$$

$$v_2' = \begin{bmatrix} v_r \\ v_r r' g + v_t \end{bmatrix} \tag{14b}$$

Moreover, since $\det J_1 = \det J_2 = 1$ for rotation, Equation (9) became an accurate result instead of an approximate one. In other words, when $\det J = 1$, the optimized transformation-mass-transfer theory became the same as the transformation-thermotics theory.[38,39]

Finally, we introduced a chemical wave separator that was designed by transforming the radius and the angle simultaneously. As illustrated by Figure 1d, mixture chemical waves of particles A and B flow in from the upper side and pass by the separator, which is denoted by grids. Then they are separated into several branches and flow out by the lower side. During this process, particles A and B are separated and converged to different regions. The following are the detailed principles for the separation.

For the sake of convenience, we divided the separator into two areas. The right-hand rectangle was marked as area-1, and the other was area-2. The length and width of area-1 were set as x_0 and y_0, respectively. Here, considering brevity and aesthetic, we operated the transformation in Cartesian coordinates. Then the coordinate transformation for A in area-1 could be expressed as $x' = (y/(2y_0) + 1) - x_0 y/(2y_0)$ and $y' = y$. Similarly, for B it became $x' - x_0 = (y/(2y_0) + 1) + x_0 y/(2y_0)$ and $y' = y$. Thus, the Jacobian matrices could be derived

$$J_{1A} = \begin{bmatrix} (y' + 2y_0) / (2y_0) & (x' - x_0) / (y' + 2y_0) \\ 0 & 1 \end{bmatrix} \tag{15a}$$

$$J_{1B} = \begin{bmatrix} (y' + 2y_0) / (2y_0) & x' / (y' + 2y_0) \\ 0 & 1 \end{bmatrix} \tag{15b}$$

where J_{1A} represents the Jacobian-transformation matrix for A in area-1, and J_{1B} represents that for B. Then according to Equation (9), we were able to determine the diffusivities $\overleftrightarrow{D}_{1A}$ and $\overleftrightarrow{D}_{1B}$ as well as the convection velocities v_{1A} and v_{1B} in area-1. As for the physical parameters in area-2, they could be naturally derived based on symmetry. The concrete values of each parameter were $x_0 = 7.5 \times 10^{-4}$ m, $y_0 = 0.007$ m, $D_{s0} = 8 \times 10^{-10}$ m s^{-1}, and $v_{s0} = [0,\ 10^{-3}]^T$ m s^{-1}. Moreover, it could be concluded from Equations (10)–(15) that the physical parameters were independent of frequencies of incident waves, which reflects one of advantages of our theory.

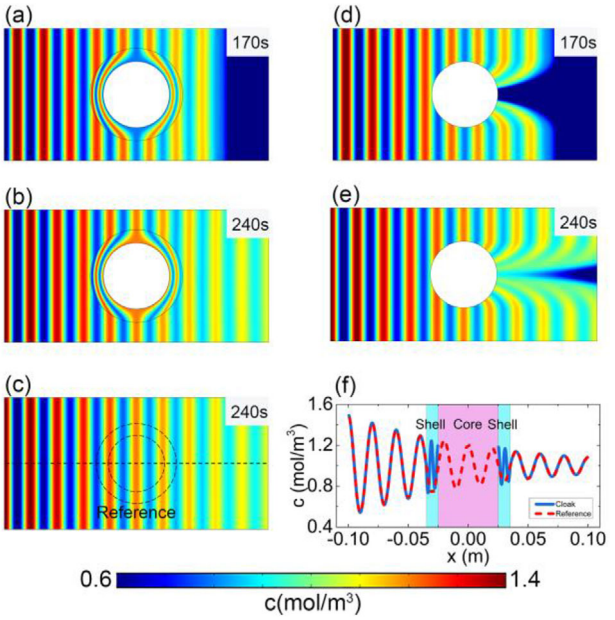

Figure 3. Simulation results of cloaking. a,b) Concentration profiles at 170 and 240 s, respectively. c) Concentration profiles in a pure background at 240 s. d,e) Concentration profiles with an obstacle at 170 and 240 s, respectively. f) Comparison between reference (c) and cloaking (b) at 240 s.

2.4. Results for Cloaking, Concentrating, and Rotating

To confirm the present theory, we utilized COMSOL Multiphysics[40] to perform finite element simulations. The boundary conditions for cloaking, concentrating, and rotating are schematically shown in Figure 1a–c, respectively. A periodic concentration source, denoted as $c_b = c_a \cos(\omega_0 t) + c_r$ where $c_a = 0.5$ mol m^{-3}, $\omega_0 = \pi/10$ s^{-1}, and $c_r = 1$ mol m^{-3}, was applied to the left boundary (the red one). According to Equation (4), the decay rate is dependent on ω. Thus we set ω_0 as $\pi/10$ s^{-1} to make a relatively low dissipation. The right boundary was set as an open boundary (the blue one). We also set isolated and no-flow conditions on the upper and lower boundaries. In Figure 1a, the inner boundary was also set with isolated and no-flow conditions. We set the diffusivity and advection velocity of the background as D_0 and v_0, respectively. All parameters were designed according to Equations (10)–(14), and the simulations of cloaking, concentrating, and rotating are exhibited in **Figures 3–5**, respectively.

In Figure 3a,b, we coated an obstacle with our designed cloak. Comparing it with Figure 3c, the concentration profiles in the background were the same, so the chemical wave was not disturbed despite the obstacle. Moreover, according to Equation (10), the tangential component of diffusivity is far larger than the radial component when $r' \sim r_1$, leading to the chemical waves bypassing the core region, which was in good agreement with the simulation results. Meanwhile, the concentration amplitude decayed as the chemical wave traveled forward, which was also

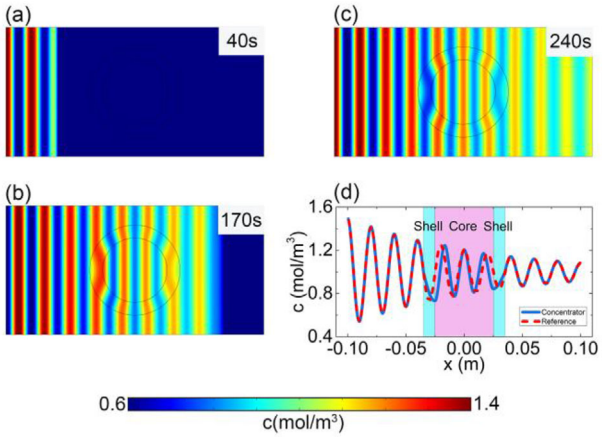

Figure 4. Simulation results of concentrating. a–c) Concentration profiles at 40, 170, and 240 s, respectively. d) Comparison between reference (Figure 3c) and concentrating (c) at 240 s.

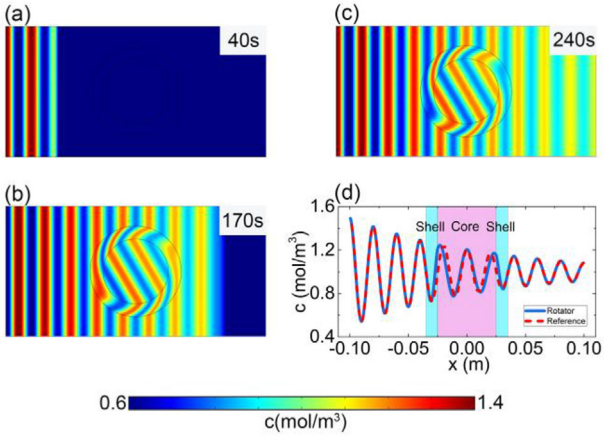

Figure 5. Simulation results of rotating. a–c) Concentration profiles at 40, 170, and 240 s, respectively. d) Comparison between reference (Figure 3c) and rotating (c) at 240 s.

consistent with our theory. However, in the absence of cloaking, the concentration wave was scattered severely when passing by the obstacle (Figure 3d,e). To discuss the cloaking effect quantitatively, we extracted the concentration values along a horizontal line in the center (the dashed line in Figure 3c). As shown in Figure 3f, the dashed line represented the concentration distribution in a pure background, and the solid line represented that with a cloak. These lines were well overlapped in the background, confirming our theory again. Moreover, the data showed that the concentration difference $|c_{\text{cloak}} - c_{\text{reference}}|$ in background was less than 0.01 mol m^{-3}, reflecting a good cloaking performance with an error of less than 1%.

The simulation results of concentrating are presented in Figure 4a–c. The concentration gradient was indeed increased in Figure 4c, which was also reflected in Figure 4d with the solid line being denser than the dashed line in the core. These results were consistent with the theoretical expectation where the coordinate transformation essentially compresses the space surrounded by the dashed circle into that by the inner circle [Figure 1b]. In addition, the concentrator also did not affect the concentration profile in the background, and the concentration difference $|c_{\text{cloak}} - c_{\text{reference}}|$ in background was still less than 0.01 mol m^{-3}, confirming the feasibility of the optimized theory.

Similarly, Figure 5a,c shows the rotating effect of a chemical wave at 40, 170, and 240 s, respectively. Obviously, the chemical wave inside the core was deflected counterclockwise by $\pi/6$ without distorting the background concentration profile. This rotation function was achieved by linearly deflecting concentric circles inside the shell, which could be reflected from the gradual deflection of the concentration profiles. Moreover, as mentioned above, the disturbance of rotating should theoretically be zero due to det $J = 1$. For comparison, Figure 5d shows the concentration distributions of a pure background and that with a rotator. Their difference was even less than 0.001 mol m^{-3}, which was ten times smaller than that of cloaking and concentrating. As a result, the proposed theory worked well in the case of transforming only the radius or only the angle.

2.5. Results for Separating

We set the diffusivity and convection velocity of the background material as D_{s0} and v_{s0}, respectively. The geometric parameters were set as m_1 and m_2. Next, we added $c_{sb} = c_{sa}\cos(\omega_{s0}t) + c_{sr}$ to the top boundary, where $c_{sa} = 0.5$ mol m^{-3}, $\omega_{s0} = \pi$ s^{-1}, and $c_{sr} = 1$ mol m^{-3}. The bottom boundary was set as open boundary. Finally, isolated and no-flow conditions were applied to the remaining sides.

Simulation results are given in **Figure 6**. The first column of figures exhibited propagation of chemical waves in a pure background medium at 6, 12, and 18 s. The second column of figures showed the propagation of particle A in a background medium with a separator. The third column of figures displayed separation results for particle B. As observed in Figure 6b1–b3,c1–c3, the chemical waves were separated into different regions without being obviously disturbed from the background wave profiles, which indicated that the phase feature was protected after the chemical waves were split by the separator. Although the separated particles would immerse into the cloaking region as time goes by, for example, particle A from both sides will gradually diffuse into the middle region, the immersion was slow when compared to the convection velocity. As reflected by the deletion of det J in Equations (9) and (15), here det J equaled $(\overleftrightarrow{\gamma}' + 2\gamma_0)/(2\gamma_0)$, which ranged from 1/2 to 1, and induced error for $\overleftrightarrow{D}_{1A}$ and $\overleftrightarrow{D}_{1B}$ as well as v_{1A} and v_{1B}, which may account for the slow immersion.

To further reveal the separation effect, we compared the particle concentration data with and without the separator. The results are presented in Figure 6, where 6(d1), 6(d2), and 6(d3) display the relation between coordinate x and concentration differential Δc at 6, 12, and 18 s, successively. The detailed values were extracted along the green dashed line ($\gamma = -0.0027$ m) in Figure 6. Here, the blue dots and red dots referred to $c_{A} - c_{\text{reference}}$ and $c_{B} - c_{\text{reference}}$, respectively. As reflected from the scatter diagrams, the differential values Δc in the convergence region for each particle were ≈0 mol m^{-3}, which was in good agreement with the previous results. Moreover, the sharp decay of the particle concentration between the convergence and

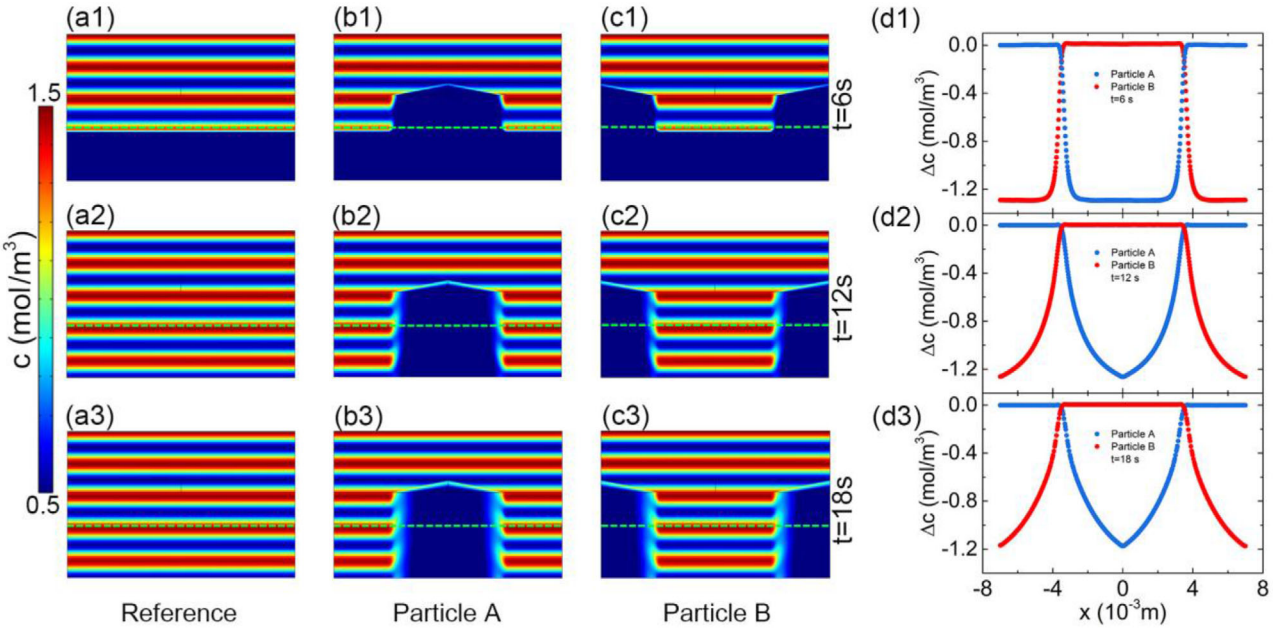

Figure 6. Simulation results of separating chemical waves composed of particles A and B, respectively. a1–a3) Propagation results of chemical waves in a pure background medium at 6, 12, and 18 s, respectively. b1–b3) Results of particle-A chemical waves in a background medium with separator at 6, 12, and 18 s, respectively. c1–c3) Results of particle-B chemical waves in a background medium with separator at 6, 12, and 18 s, respectively. d1) Particle A's [or Particle B's] concentration difference Δc between (b1) and (a1) [or between (c1) and (a1)] along x axis at 6 s, according to the data extracted from the x-directed green dashed lines in (b1) and (a1) [or in (c1) and (a1)]. Similarly, (d2) and (d3) show Δc at 12 and 18 s, respectively.

cloaking regions provided a demonstration of well-performed particle separation. Hence, the optimized transformation theory still performed well when transforming both the radius and angle.

3. Conclusion

We have demonstrated a good performance of four functional devices for controlling dynamic concentration profiles based on the optimized transformation-mass-transfer theory. These results have potential applications in some practical fields, such as tracing biochemical-particle concentrations where a detector might receive pulse-like or wave-like signals, cloaking an area to block chemical leaks that are harmful to the environment and creatures, and separating toxic gases (such as CO) and O_2 when gas leaks happen. Particularly, in spite of various existing separation methods,[41] the preservation of the phase feature was ignored. Different from the past studies,[11,42] we considered the diffusion together with convection so that the harmonic concentration source could be applied. And thus the proposed separator could separate wave-form chemical diffusion without changing the phase feature. As a result, the proposed theory is of practical value for controlling chemical waves.

For experimental demonstration, these devices could be fabricated with a porous media to control diffusivity.[43–45] Here we provided a brief suggestion for experimental fabrication. According to the effective medium theory, the complicated diffusivities and convection velocity could be possibly achieved by several common materials.[13] Taking the separator as an example, in Ref. (13), the diffusivity is independent on spatial position, so only one constant rotating angle is needed. However, in our work, the diffusivity varied with different position. Thus the distribution of rotating angle was more complicated. In spite of anisotropy and inhomogeneity, the transformed physical parameters could be reproduced by multilayer structures rotated by different angles with respect to x-axis. As shown in **Figure 7**, the separator was divided into many rectangular pieces. We set the diffusivity of the piece center as that of the whole piece, which could be obtained by Equations (9) and (15) in this paper. Then every small rectangle could be further divided into different isotropic materials. Each of pieces consists of four different materials with a special rotating angle which could refer to Equations (6) and (7) in Ref. (13). Let us focus on one of the pieces enlarged by dashed box in the inset of Figure 7. Four materials were denoted as material M_1, M_2, N_1, and N_2, respectively. And their diffusivities for particle A and B were set as: $D_A = D_M$ and $D_B = D_1$ for material M_1, $D_A = D_M$ and $D_B = D_2$ for material M_2, $D_A = D_N$ and $D_B = D_1$ for material N_1, and $D_A = D_N$ and $D_B = D_2$ for material N_2. The values of D_M, D_N, D_1, and D_2 were determined according to the

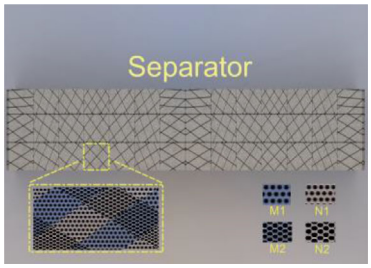

Figure 7. Experimental suggestion. Schematic diagram of separator designed by using the effective medium theory.

effective medium theory and Equation (9). It should be noted that the rotating angles and diffusivities vary with different species. Thus, the control of diffusivities became possible. In addition, with recent efforts to control hydrodynamic fields,[34,46–48] advection velocity could also be manipulated in principle, such as using electro-osmosis.[48] We assumed the same chemical species solubilities for brevity and ignored chemical potentials that might be the major driving forces in concentrated solutions. These assumptions were also reasonable because the transformation theory still revealed promising performance when species solubilities and chemical potentials were considered.[12]

In summary, we have established a model to describe chemical waves and discuss their propagation properties. Compared with steady state, the governing equation of transient mass transfer is not form-invariant under the coordinate transformation, which makes it distinctly different. To solve the problem, we proposed an optimized transformation transient-mass-transfer theory and further designed four functional devices to flexibly control chemical waves. These results have potential applications to control transient mass transfer in various biochemical systems, such as tracing medicine particles and preventing chemical leaks. It was also promising for revealing more physical properties based on the model of chemical waves like geometric phases,[49,50] diffusion behavior in nanoscale,[51,52] and symmetry breaking.[53]

Acknowledgements

The authors acknowledge financial support from the National Natural Science Foundation of China under Grants Nos. 11725521 and 12035004 and from the Science and Technology Commission of Shanghai Municipality under Grant No. 20JC1414700.

Conflict of Interest

The authors declare no conflict of interest.

Data Availability Statement

Data available on request from the authors.

Keywords

chemical wave, cloak, concentrator, separator, transformation theory

Received: September 6, 2021
Revised: October 26, 2021
Published online: November 18, 2021

[1] W. J. Koros, C. Zhang, *Nat. Mater.* **2017**, *16*, 289.
[2] M. J. Xuan, J. X. Shao, J. Zhao, Q. Li, L. R. Dai, J. B. Li, *Angew. Chem. Int. Ed.* **2018**, *57*, 6049.
[3] S. M. Rajput, S. Kumar, V. K. Aswal, O. A. El Seoud, N. I. Malek, S. K. Kailasa, *ChemPhysChem* **2018**, *19*, 865.
[4] X. L. Chen, L. Wu, H. M. Yang, Y. Qin, X. H. Ma, N. W. Li, *Angew. Chem. Int. Ed.* **2021**, *60*, 17875.
[5] D. S. Sholl, R. P. Lively, *Nature* **2016**, *532*, 435.
[6] H. Z. Sun, Y. K. Ren, L. K. Hou, Y. Tao, W. Y. Liu, T. Y. Jiang, H. Y. Jiang, *Anal. Chem.* **2019**, *91*, 5729.
[7] M. Piechowicz, R. Chiarizia, S. Skanthakumar, S. J. Rowan, L. Soderholm, *ChemPhysChem* **2020**, *21*, 1157.
[8] A. Fick, *J. Membr. Sci.* **1995**, *100*, 33.
[9] E. L. Cussler, *Diffusion: Mass Transfer in Fluid Systems*, Cambridge University, New York **2009**.
[10] S. Guenneau, T. M. Puvirajesinghe, *J. R. Soc. Interface* **2013**, *10*, 20130106.
[11] J. M. Restrepo-Flórez, M. Maldovan, *Sci. Rep.* **2016**, *6*, 21971.
[12] J. M. Restrepo-Flórez, M. Maldovan, *Appl. Phys. Lett.* **2017**, *111*, 071903.
[13] J. M. Restrepo-Flórez, M. Maldovan, *J. Phys. D: Appl. Phys.* **2017**, *50*, 25104.
[14] L. Yang, C. B. Liu, Y. Bai, L. J. Qiao, J. Zhou, *Adv. Theory Simul.* **2018**, *1*, 1700004.
[15] R. Kapral, K. Showalter, *Chemical Waves and Patterns*, Springer, Dordrecht **1995**.
[16] O. Steinbock, P. Kettunen, K. Showalter, *J. Phys. Chem.* **1996**, *100*, 18970.
[17] V. E. Deneke, S. Di Talia, *J. Cell Biol.* **2018**, *217*, 1193.
[18] F. Avanzini, G. Falasco, M. Esposito, *J. Chem. Phys.* **2019**, *151*, 234103.
[19] R.-F. Cui, Q.-H. Chen, J.-X. Chen, *Nanoscale* **2020**, *12*, 12275.
[20] S. Thakur, J. X. Chen, R. Kapral, *Angew. Chem. Int. Ed.* **2011**, *50*, 10165.
[21] A. Adamatzky, M. A. Tsompanas, T. C. Draper, C. Fullarton, R. Mayne, *ChemPhysChem* **2020**, *21*, 90.
[22] H. N. Luo, C. L. Wang, L. Ren, Q. Y. Gao, C. W. Pan, I. R. Epstein, *Angew. Chem. Int. Ed.* **2016**, *55*, 4988.
[23] I. S. Proskurkin, P. S. Smelov, V. K. Vanag, *ChemPhysChem* **2019**, *20*, 2162.
[24] R. Schittny, A. Niemeyer, M. Kadic, T. Bückmann, A. Naber, M. Wegener, *Optica* **2015**, *2*, 84.
[25] L.-J. Xu, J.-P. Huang, *Chin. Phys. Lett.* **2020**, *37*, 120501.
[26] S. Yang, J. Wang, G. L. Dai, F. B. Yang, J. P. Huang, *Phys. Rep.* **2021**, *908*, 1.
[27] B. Orazbayev, M. Beruete, A. Martínez, C. García-Meca, *Phys. Rev. A* **2016**, *94*, 063850.
[28] S. Guenneau, A. Diatta, T. M. Puvirajesinghe, M. Farhat, *J. Opt.* **2017**, *19*, 103002.
[29] S. Schmidt, P. Ortoleva, *J. Chem. Phys.* **1977**, *67*, 3771.
[30] H. Kitahata, R. Aihara, N. Magome, K. Yoshikawa, *J. Chem. Phys.* **2002**, *116*, 5666.
[31] H. Kitahata, N. Yoshinaga, K. H. Nagai, Y. Sumino, *Phys. Rev. E* **2011**, *84*, 015101.
[32] R. Schittny, M. Kadic, S. Guenneau, M. Wegener, *Phys. Rev. Lett.* **2013**, *110*, 195901.
[33] S. Zhang, C. G. Xia, N. Fang, *Phys. Rev. Lett.* **2011**, *106*, 024301.
[34] J. Park, J. R. Youn, Y. S. Song, *Phys. Rev. Lett.* **2019**, *123*, 074502.
[35] G. Fujii, T. Ueta, *Phys. Rev. E* **2016**, *94*, 043301.
[36] Z.-X. Xu, H. Gao, Y.-J. Ding, J. Yang, B. Liang, J.-C. Cheng, *Phys. Rev. Appl.* **2020**, *14*, 054016.
[37] G. Fujii, M. Takahashi, Y. Akimoto, *Appl. Phys. Lett.* **2021**, *118*, 101102.
[38] J. P. Huang, *Theoretical Thermotics: Transformation Thermotics and Extended Theories for Thermal Metamaterials*, Springer, Singapore **2020**.
[39] L. J. Xu, S. Yang, G. L. Dai, J. P. Huang, *ES Energy Environ.* **2020**, *7*, 65.
[40] http://www.comsol.com/ (accessed: 2021).
[41] B. Çetin, M. B. Özer, M. E. Solmaz, *Biochem. Eng. J.* **2014**, *92*, 63.
[42] X. Zhou, G. Q. Xu, H. Y. Zhang, *Compos. Struct.* **2021**, *267*, 113866.
[43] Y. X. Zhang, L. P. Liu, *Am. J. Sci.* **2012**, *312*, 1028.
[44] I. V. Belova, G. E. Murch, *J. Phys. Chem. Solids* **2003**, *64*, 873.
[45] C. D. V. Siclen, *J. Phys. Chem. Solids* **2004**, *65*, 1199.
[46] J. Park, J. R. Youn, Y. S. Song, *Phys. Rev. Appl.* **2019**, *12*, 061002.
[47] W.-S. Yeung, V.-P. Mai, R.-J. Yang, *Phys. Rev. Appl.* **2020**, *13*, 064030.

[48] E. Boyko, V. Bacheva, M. Eigenbrod, F. Paratore, A. D. Gat, S. Hardt, M. Bercovici, *Phys. Rev. Lett.* **2021**, *126*, 184502.
[49] D. F. Yuan, Y. F. Guan, W. T. Chen, H. L. Zhao, S. R. Yu, C. Luo, Y. X. Tan, T. Xie, X. A. Wang, Z. G. Sun, D. H. Zhang, X. M. Yang, *Science* **2018**, *362*, 1289.
[50] L. J. Xu, G. L. Dai, G. Wang, J. P. Huang, *Phys. Rev. E* **2020**, *102*, 032140.
[51] G. X. Nie, J. Y. Huang, J. P. Huang, *J. Phys. Chem. B* **2016**, *120*, 9011.
[52] T. Qiu, X. W. Meng, J. P. Huang, *J. Phys. Chem. B* **2015**, *119*, 1496.
[53] Y. Li, Y.-G. Peng, L. Han, M.-A. Miri, W. Li, M. Xiao, X.-F. Zhu, J. L. Zhao, A. Alù, S. H. Fan, C.-W. Qiu, *Science* **2019**, *364*, 170.